

Peculiar polarization response in chiral liquid crystal stacks for multispectral camouflage

ZIQIAN HE, KUN YIN, AND SHIN-TSON WU* 

College of Optics and Photonics, University of Central Florida, Orlando, Florida 32816, USA

*swu@creol.ucf.edu

Abstract: Chiral liquid crystals are self-organized Bragg reflectors which respond to circularly polarized light. Manipulation of the chiral structure has aroused great research interest. The x - y plane two-dimensional patterning of chiral liquid crystals leads to reflective planar optics, and the z -axis modulation results in a variety of photonic bandgap controls. Here, the optical properties of even-number left- and right-handed chiral liquid crystal stacks are investigated, with emphasis on the linear polarization response. Under certain conditions, a linearly polarized incidence can result in a linearly polarized reflected light. More intriguingly, the linear polarization has different forms of response to thick and thin chiral liquid crystal sublayers and responds to the rotation of liquid crystal alignment. Based on the peculiar polarization response, a new type of wavelength-response camouflage and anti-counterfeiting is conceptually proposed, which can hide two different images simultaneously within a small spectral range. Our work paves the way for three-dimensional manipulation of chiral liquid crystals and enlightens novel applications.

© 2021 Optical Society of America under the terms of the [OSA Open Access Publishing Agreement](#)

1. Introduction

Chiral nematic liquid crystal, also termed cholesteric liquid crystal (CLC), is formed by self-organized rod-like molecules with continuously rotating directors. The periodic helical structure forms a chiral Bragg grating, which reflects circularly polarized light with the same handedness as the helix. Its photonic bandgap central wavelength, and bandwidth can be estimated by $(n_o+n_e)p/2$ and $(n_o-n_e)p$, respectively, where n_o and n_e are the ordinary and extraordinary refractive indices, and p is the helix pitch [1]. Ascribed to its circular polarization selectivity and photonic bandgap, CLC can be utilized as circular polarizers, color filters, and reflective decoration coatings [2–7]. During past decades, plethora of works explored optical properties of CLC in different spatial dimensions and brought new insights to this special liquid crystalline phase. Studies on two-dimensional (2D) patterning in x - y plane led to patterned CLC-based planar optics, where high quality and tunable reflective optical devices have been demonstrated [8–15]. Meanwhile, efforts have also been made to engineer its structure in z -axis. By inserting defect layers into the helical periodic structure, band splitting can be rationally designed, and special polarization properties have been observed [16–19].

In this work, we revisit the optical properties of even-number left- and right-handed CLC layers stack and emphasize their linear polarization response. It was previously found that for an even number of sublayers, the eigen polarizations of the system are degenerate [19]. Through numerical simulation, the eigen polarization degeneracy was validated for cases where each CLC sublayer rotates by integer multiples of π . However, the eigen polarization degeneracy can be broken in other cases. More importantly, for cases where each CLC sublayer rotates by integer multiples of π , upon linear polarization incidence, reflected light in the photonic bandgaps turns to be linearly polarized. For a thick CLC sublayer, the linear polarization is rotated continuously within the photonic bandgap. For a thin CLC sublayer, the bandgap splits into several bandgaps, but still maintains a linearly reflected light. Particularly, the polarization of reflected light at the central bandgap is perpendicular to the polarization of reflected light at the side bandgaps. We show that this can be understood by scrutinizing phase of reflected circularly polarized light.

Further characterizations manifest that upon rotating linear analyzer or liquid crystal alignment, the reflection spectrum will change accordingly. Inspired by this peculiar linear polarization response, we propose a new type of wavelength-response camouflage and anti-counterfeiting. By encrypting the message in liquid crystal alignment layer, the information can only be extracted by the incident light within the photonic bandgap. Excitingly, two different images can be extracted by varying the probing wavelength. Our work not only discovers special optical properties of CLC stacks, but also sheds light on full three-dimensional design of chiral liquid crystals.

2. Results and discussion

2.1. Cholesteric liquid crystal stack

Figure 1(a) illustrates a schematic of CLC stack studied in this work. The CLC stack consists of alternating left-handed and right-handed CLC helical sublayers where the total number of sublayers is the same for left and right handedness. In this structure, the repeating unit is a left-handed and a right-handed CLC sublayer. Within each unit, the liquid crystal directors first continuously rotate by $2m\pi$ (left-hand), and then rotate backwards by $2m\pi$ (right-hand). Such a unit repeats n times along z -axis to ensure a well-established Bragg reflection.

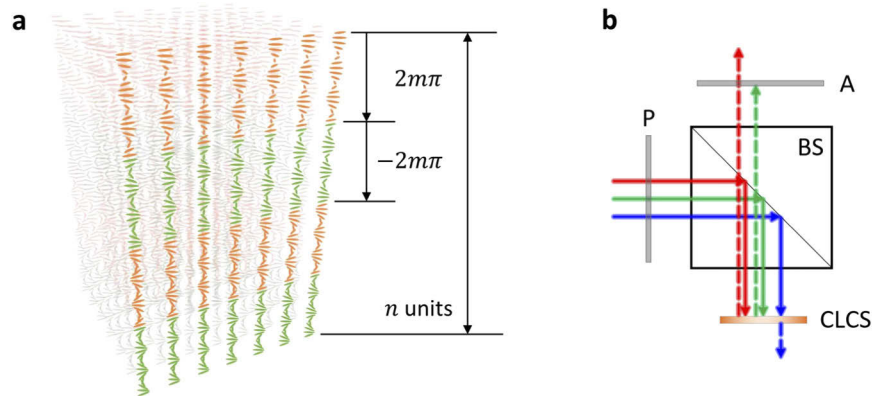


Fig. 1. (a) Schematic illustration of a CLC stack (CLCS). Each repeating unit consists of a left-handed CLC sublayer with a total director rotation angle of $2m\pi$ and a right-handed CLC sublayer with a total director rotation angle of $-2m\pi$. In the graph, $m = 1.5$ and $n = 2$. (b) Optical setup for numerical simulation. A white light first passes through a polarizer (P) and is directed by the beam splitter (BS) to the CLC stack. Upon Bragg reflection, the reflected light is further filtered by an analyzer (A).

The numerical simulation setup is plotted in Fig. 1(b). A polarized (either linear or circular) white light is incident on the CLC stack. Upon reflection, an analyzer (either linear, circular, or non-polarized) is used to filter the reflected light. The optical response of the CLC stack is simulated by a homemade 4-by-4 Berreman matrix solver [20] loaded in MATLAB. The step-by-step formula of the 4-by-4 Berreman matrix method used in this paper can be found in [21]. The nematic liquid crystal material is a reactive mesogen (RM 257, Merck). Its ordinary refractive index is assumed to be 1.52 and its birefringence is estimated by the single-band birefringence dispersion equation [22]:

$$\Delta n = G \frac{\lambda^2 \lambda^{*2}}{\lambda^2 - \lambda^{*2}}, \quad (1)$$

where $G = 2.4 \mu\text{m}^{-2}$ is a proportionality constant and $\lambda^* = 231.5 \text{ nm}$ is the mean resonance wavelength. The helical twisting pitch of both left-handed and right-handed CLCs is 410 nm. The

helix of first sublayer (from the direction of incident light) is left-handed. The CLC alignment is homogeneous unless otherwise stated.

2.2. Optical response of various CLC stack structures

The simulated reflection spectra of a white light incidence upon various CLC stack structures are shown in Fig. 2. The incident polarization is linear and is parallel to the liquid crystal alignment direction. Different analyzers, including circular, linear, and non-polarized, are applied to characterize the polarization properties of reflected light. There are several implications from the results: 1) For cases where each CLC sublayer rotates by integer multiples of π , the reflected light is linearly polarized. It means the two circular polarizations are degenerate, which can be noticed from Fig. 2 that their reflectance is similar. However, the degeneracy can collapse when the condition is not met. Apparently, in the case of $m = 1.25$ and $n = 8$, the reflected light is not linearly polarized within side bandgaps. 2) For a thick CLC sublayer, Bragg reflection is well established within the sublayer and thus no band splitting is observed. Nevertheless, the reflected linear polarization is continuously rotated within the bandgap. 3) For a thin CLC sublayer, the photonic bandgap splits, but the central bandgap stays. The side bandgaps shift away from the central bandgap when the CLC sublayer is thinner. The linear polarization of reflected light from central bandgap is perpendicular to that of reflected light from side bandgaps.

To understand the linear polarization response of CLC stacks, another group of simulation is performed for the case of $m = 10$, $n = 1$. The incident polarization is now circularly polarized, and the analyzer has the same circular polarization as the input light. Figure 3(a) and 3(b) show the reflection spectrum (colored solid line) and phase (orange dots) of left-handed circularly polarized (LCP) and right-handed circularly polarized (RCP) input light, respectively. The reflection spectrum without an analyzer is also drawn as a black dashed line for reference. From Fig. 3, the reflected light with circularly polarized input maintains its original circular polarization (Photon spin is flipped since the propagation direction is reversed). Interestingly, the reflection phase variation of LCP input within the photonic bandgap is much slower than that of RCP input. This can be interpreted as the result of optical path difference between the two circular polarizations. In our simulation, since the first CLC layer is left-handed, the LCP input light will be reflected by the first CLC layer. By contrast, the RCP input light will be reflected by the second CLC layer. Therefore, RCP light has a longer traveling distance which will result in an extra dynamic phase accumulation.

Similar simulation is performed for the case of $m = 1$, $n = 10$ as well, and results are plotted in Fig. 4. For the central bandgap (~ 653 nm), the two circularly polarized reflected lights are in phase, while they are 180° out of phase for the side bandgap (~ 524 nm). The different phase behavior in central and side bandgaps is the reason for the orthogonal linear polarization directions. However, in this case, since each sublayer is thin, the phase difference needs to be understood by taking multilayer interference into account.

2.3. Influence of linear analyzer and liquid crystal alignment direction

In this subsection, we further explore the influence of linear analyzer and liquid crystal alignment direction. Here, a CLC stack with $m = 1$, $n = 10$ is taken as an example, and the input light is linearly polarized at 0° . To study the impact of linear analyzer, the liquid crystal alignment is set along 0° and the reflection spectrum with a rotating analyzer is recorded. As shown in Fig. 5(a), upon analyzer rotation, reflection intensity of the central bandgap decreases and that of the side bandgap increases. It leads to a perceived color shift from red, via yellow, to green, as depicted in CIE 1931 color space. When the analyzer is rotated 90° , the central bandgap reaches minimum reflection intensity. To study the impact of liquid crystal alignment, the analyzer is fixed at 0° , and the CLC stack is rotated. As demonstrated in Fig. 5(b), similar color shift trend is observed. On the other hand, spectral intensity modulation in thick CLC stacks (e.g. $m = 10$, $n = 1$) by

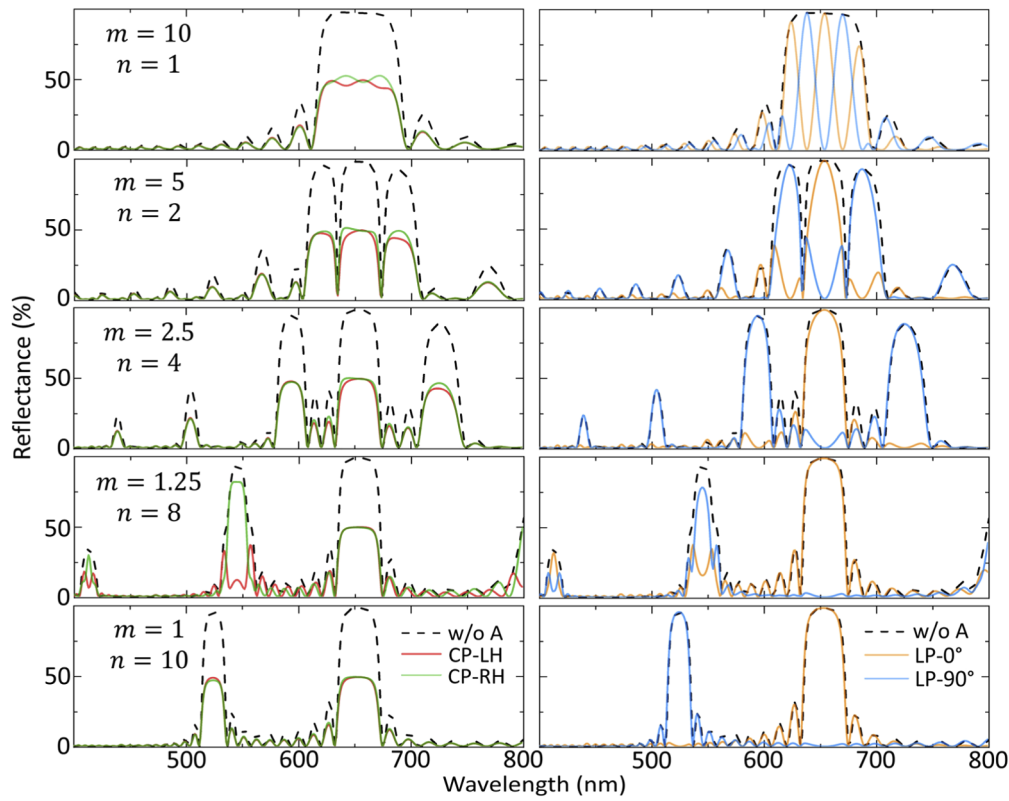


Fig. 2. Reflection spectra of various CLC stack under different analyzers where the incident light is linearly polarized (0°). Plots in the same row denotes the results for the same CLC stack structure. Left and right columns show the results of circularly and linearly polarized analyzers, respectively. The reflection spectrum without an analyzer is plotted in black dashed lines as a reference. Red, green, yellow, cyan solid lines stand for the results of using left-handed circular, right-handed circular, 0° linear, 90° linear analyzers, respectively. w/o A: without analyzer; CP: circular polarization; LH: left-handed; RH: right-handed; LP: linear polarization.

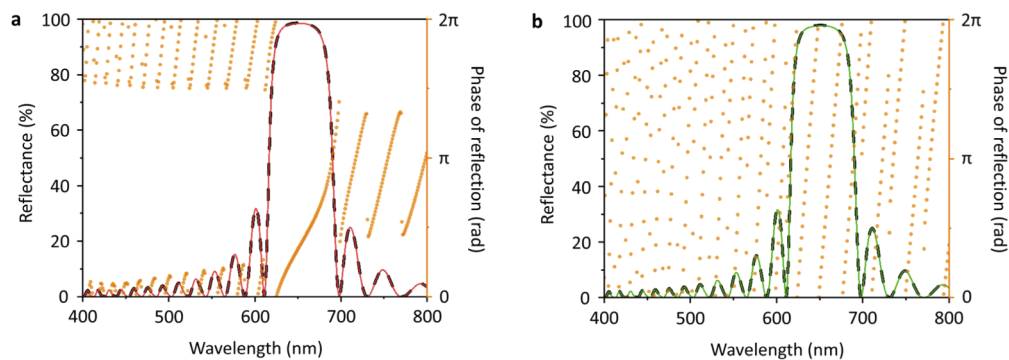


Fig. 3. Reflection spectra and phase of a CLC stack with $m = 10$, $n = 1$. The incident light is (a) LCP and (b) RCP. Red and green solid lines denote the reflection spectrum with a left-handed and a right-handed circular analyzer. Black dashed line denotes the reflection spectrum without an analyzer. Phase of reflection is marked as yellow dots.

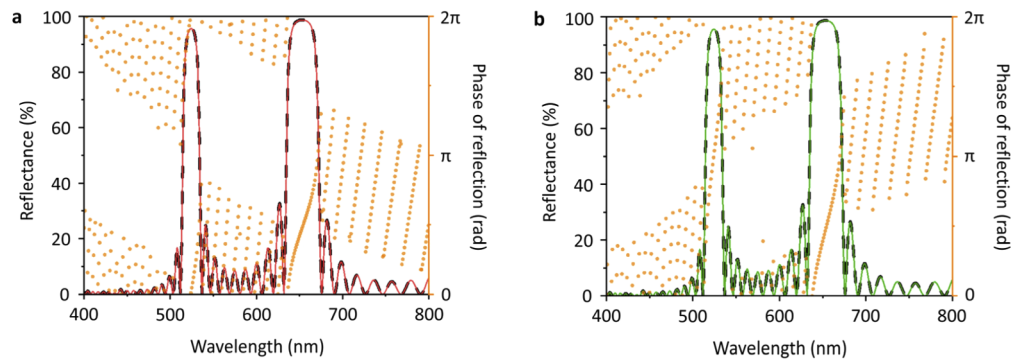


Fig. 4. Reflection spectra and phase of a CLC stack with $m = 1$, $n = 10$. The incident light is (a) LCP and (b) RCP. Red and green solid lines denote the reflection spectrum with a left-handed and a right-handed circular analyzer. Black dashed line denotes the reflection spectrum without an analyzer. Phase of reflection is marked as yellow dots.

rotating a linear analyzer or alignment direction can also be expected. However, the reflected color will have minor changes because the bandgap is fixed at red wavelengths. For stacks with thin CLC sublayers, the highly saturated colors as well as the ability of color patterning are very practical for encoding color images, comparing to polarization-dependent color generation by dielectric metasurfaces [23,24].

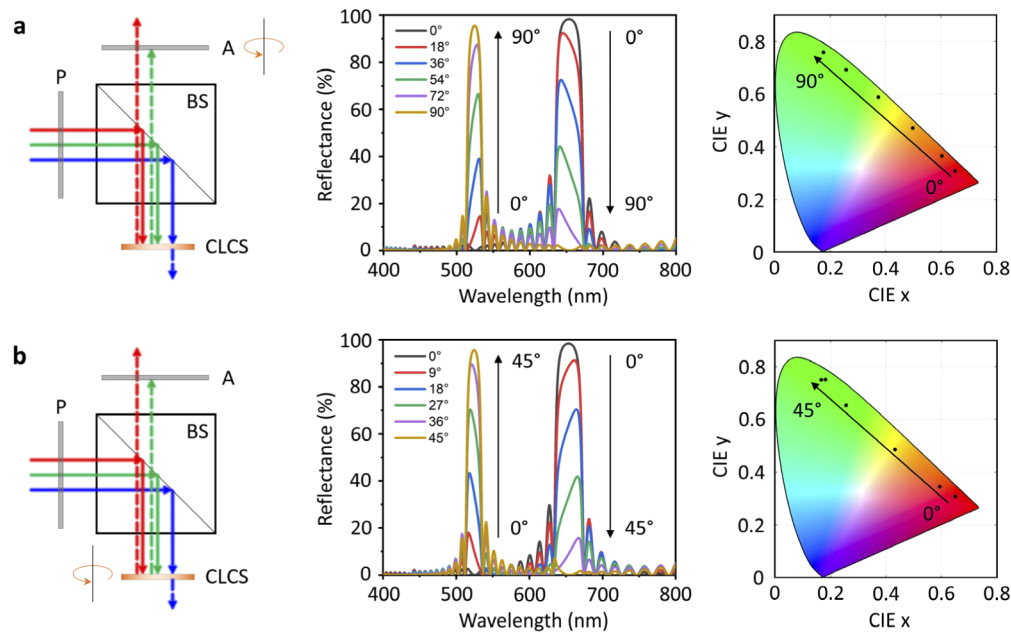


Fig. 5. Influence of rotating (a) the linear analyzer and (b) the CLC stack. The input light is linearly polarized at 0° , and the structure of CLC stack is $m = 1$, $n = 10$. (a, b) Left shows the schematic of simulation. Middle demonstrates the calculated reflection spectra upon analyzer/CLC stack rotation. Right depicts the corresponding color shift of the reflection spectra in CIE 1931 color space. P, polarizer; A, analyzer; BS, beam splitter; CLCS, CLC stack.

From Fig. 5, the liquid crystal alignment direction only needs 45° rotation to realize 90° linear polarization rotation of the reflected light. It indicates that the phase of reflection for circularly polarized input light depends on the liquid crystal alignment direction. To better understand how the liquid crystal alignment direction affects the phase of reflection in this case, we extract the phase of circularly polarized reflected light within the two bandgaps. Figure 6(a) and 6(b) exhibit the phase of reflection for $\lambda = 524$ nm and $\lambda = 653$ nm, respectively. With rotating alignment direction, phase of left-handed reflected light for the two wavelengths is decreasing while that of right-handed reflected light keeps increasing. Comparing the central wavelengths of the two bandgaps, LCP and RCP lights show a constant $\pm 90^\circ$ out-of-phase, respectively. This is the root cause of linear polarization rotation when the CLC stack is rotated.

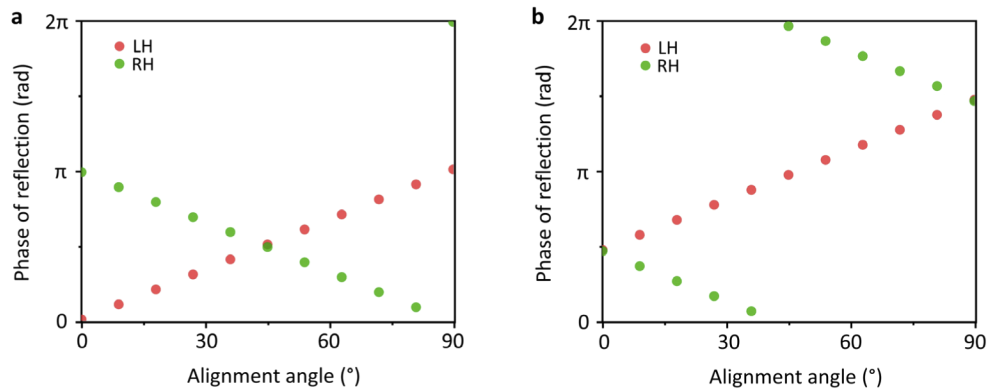


Fig. 6. Extracted phase of circularly polarized reflection for a CLC stack with $m = 1$, $n = 10$. (a) The wavelength is 524 nm, which corresponds to the side bandgap. (b) The wavelength is 653 nm, which corresponds to the central bandgap. LH: left-handed; RH: right-handed.

2.4. Multispectral camouflage enabled by 2D patterned CLC stacks

Based on the peculiar linear polarization response of CLC stacks, we conceptually propose a new type of wavelength-response camouflage and anti-counterfeiting. Previous works have been done in spatial and angular domains to create multiple images in one device [25–27]. There are also other attempts to hide an image in certain spectral range [28]. Although complex photonic structures can be and have been designed, hiding different images simultaneously within a small spectral range is still an untouched area. Inspiringly, this can be realized by the patterned CLC stacks.

Figure 7(a) shows the schematic of how to probe the images with varying wavelengths. A laser beam is first filtered by a linear polarizer (here assumed at 0°), and then hits on a patterned CLC stack. Upon Bragg reflection, the reflected light is further filtered by a linear analyzer (here assumed at 0°) and is received by the observer. To demonstrate the working principle, let us first look at the reflectance variation as a function of liquid crystal alignment direction for two wavelength channels ($\lambda_1 = 646$ nm, $\lambda_2 = 654$ nm). From Fig. 7(b), the *calculated* reflectance of a CLC stack ($m = 10$, $n = 1$) follows Malus law for both wavelengths, but there is an $1/4$ period phase shift. From Fig. 7(b), four alignment states are extracted, denoted as 1, 2, 3, 4 in the figure. State 1 shows low reflectance for λ_1 but high reflectance for λ_2 ; State 2 has low reflectance for both λ_1 and λ_2 ; State 3 exhibits high reflectance for λ_1 and low reflectance for λ_2 ; State 4 manifests high reflectance for both λ_1 and λ_2 . With these states, a high reflectance of λ_2 can correspond to an either high or low reflectance of λ_1 , and vice versa. Thus, two completely independent images can be assigned to λ_1 and λ_2 , respectively. Meanwhile, ascribed to the photonic bandgap of the CLC stack, only those wavelengths located within the bandgap will be reflected. Consequently,

the encoded information is hidden in the photonic bandgap, and different images can be extracted with different probing wavelengths, as illustrated in Fig. 7(c). For example, two different graphs are respectively encrypted to the two wavelength channels, as Fig. 7(d) shows. However, they have the same liquid crystal alignment patterns, as can be seen from the inset which depicts the alignment directions of selected area.

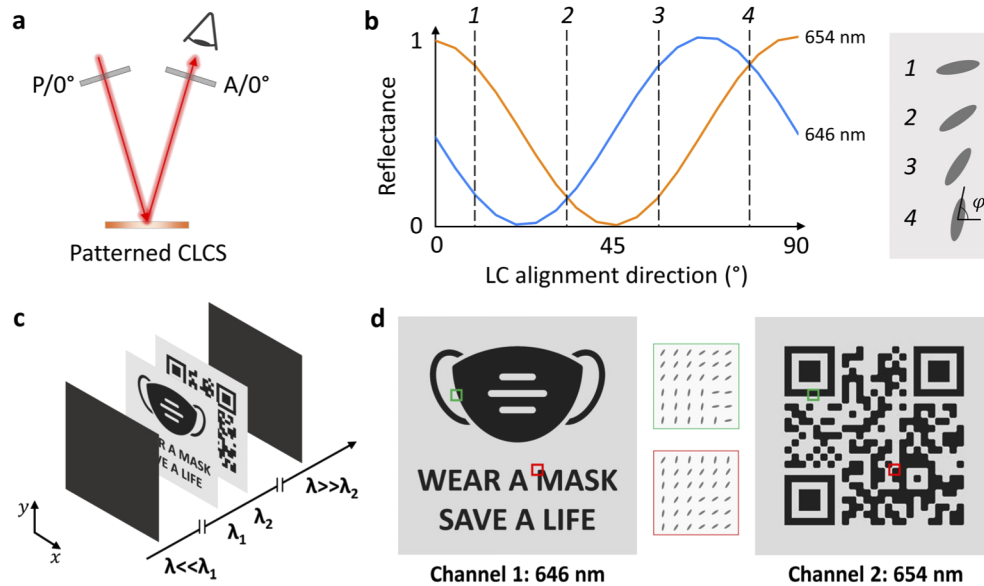


Fig. 7. Application concept demonstration of 2D patterned CLC stack in wavelength-response camouflage and anti-counterfeiting. (a) Schematic of the application usage. A laser beam filtered by a linear polarizer (0°) is incident on the patterned CLC stack. Upon Bragg reflection, observer can see different images through a linear analyzer (0°) with various laser wavelength. (b) Reflectance of two wavelength channels ($\lambda_1 = 646$ nm, $\lambda_2 = 654$ nm) as a function of liquid crystal alignment direction for a CLC stack with $m = 10$, $n = 1$. Four states are chosen for generating alignment patterns: 1. λ_1 low reflectance, λ_2 high reflectance; 2. λ_1, λ_2 low reflectance; 3. λ_1 high reflectance, λ_2 low reflectance; 4. λ_1, λ_2 high reflectance. (c) Illustration of the proposed multispectral camouflage. When incident wavelength is out of the photonic bandgap, the reflectance is negligible, and no image is shown to the observer. Within the photonic bandgap, two different images can be observed by tuning the probing laser wavelength. (d) Two different images are encrypted to two spectral channels, while they have the same liquid crystal alignment pattern. The inset highlights the alignment direction of selected area.

The images shown in the example are encoded with binary gray levels (low & high). However, other gray levels can also be created, using the strategy of duty cycle control within a pixel, similar to gray level generation in printers. Moreover, the spectral range of image hiding can be easily engineered, by choosing different helical pitch of CLCs. With this strategy, the encrypted information will be even more secure.

Here only a concept is proposed. To realize this concept, there are two critical steps. First, the desired liquid crystal alignment pattern needs to be generated on a substrate (x - y plane modulation). This step can be achieved by the well-established photoalignment technique [29]. For example, a spatial light modulator-assisted projection exposure setup can be applied to create a variety of patterns [30]. Second, the chiral liquid crystal stacks need to be formed and well-aligned on top of the substrate (z -axis modulation). Such stacks can be fabricated by spin-coating liquid crystal monomer mixtures in a layer-by-layer manner, as reported in [31,32].

However, this can be a time-consuming process since a recipe needs to be developed for precise thickness control of each sublayer.

3. Conclusion

We investigated the optical properties of even-number left- and right-handed CLC layers stack. Through numerical simulation, we show that if each sublayer is rotated by integer multiples of π , a linearly polarized input light will result in linearly polarized output. For thick CLC sublayers, the output linear polarization is continuously rotated inside the photonic bandgap. For thin CLC sublayers, the photonic bandgap is split. Particularly, the polarization of reflected light at the central bandgap is perpendicular to that of reflected light at the side bandgaps. The linear polarization response can be understood by scrutinizing phase of reflected circularly polarized light. Moreover, we demonstrate that the reflected spectrum and thus color can be managed by rotating either a linear analyzer or liquid crystal alignment. Based on this peculiar linear polarization response, a new type of wavelength-response camouflage and anti-counterfeiting is conceptually proposed. The proposed method can hide different images simultaneously within a small spectral range and the encoded wavelengths can be easily designed and engineered, owing to the self-assembly nature of CLC. Our work enables novel applications and paves the way for full three-dimensional engineering of chiral liquid crystals.

Funding. Air Force Office of Scientific Research (FA9550-14-1-0279).

Disclosures. The authors declare no conflicts of interest.

References

1. P. Yeh and C. Gu, *Optics of Liquid Crystal Displays* (Wiley, 2009).
2. Y. C. Lin, P. C. Wu, and W. Lee, "Frequency-modulated textural formation and optical properties of a binary rod-like/bent-core cholesteric liquid crystal," *Photonics Res.* **7**(11), 1258–1265 (2019).
3. P. Zhang, A. J. Kragt, A. P. Schenning, L. T. de Haan, and G. Zhou, "An easily coatable temperature responsive cholesteric liquid crystal oligomer for making structural colour patterns," *J. Mater. Chem. C* **6**(27), 7184–7187 (2018).
4. J. Zou, E. L. Hsiang, T. Zhan, K. Yin, Z. He, and S. T. Wu, "High Dynamic Range Head-up Display," *Opt. Express* **28**(16), 24298–24307 (2020).
5. R. A. M. Hikmet and H. Kemperman, "Electrically switchable mirrors and optical components made from liquid-crystal gels," *Nature* **392**(6675), 476–479 (1998).
6. N. Tamaoki, "Cholesteric liquid crystals for color information technology," *Adv. Mater.* **13**(15), 1135–1147 (2001).
7. Z. He, H. Chen, Y. H. Lee, and S. T. Wu, "Tuning the correlated color temperature of white light-emitting diodes resembling Planckian locus," *Opt. Express* **26**(2), A136–A143 (2018).
8. J. Kobashi, H. Yoshida, and M. Ozaki, "Planar optics with patterned chiral liquid crystals," *Nat. Photonics* **10**(6), 389–392 (2016).
9. J. Kobashi, H. Yoshida, and M. Ozaki, "Polychromatic optical vortex generation from patterned cholesteric liquid crystals," *Phys. Rev. Lett.* **116**(25), 253903 (2016).
10. R. Barboza, U. Bortolozzo, M. G. Clerc, and S. Residori, "Berry phase of light under Bragg reflection by chiral liquid-crystal media," *Phys. Rev. Lett.* **117**(5), 053903 (2016).
11. M. Rafayelyan and E. Brasselet, "Bragg-Berry mirrors: reflective broadband q-plates," *Opt. Lett.* **41**(17), 3972–3975 (2016).
12. P. Chen, L. L. Ma, W. Duan, J. Chen, S. J. Ge, Z. H. Zhu, M. J. Tang, R. Xu, W. Gao, T. Li, W. Hu, and Y. Q. Lu, "Digitalizing self-assembled chiral superstructures for optical vortex processing," *Adv. Mater.* **30**(10), 1705865 (2018).
13. K. Yin, Z. He, and S. T. Wu, "Reflective polarization volume lens with small f-number and large diffraction angle," *Adv. Opt. Mater.* **8**(11), 2000170 (2020).
14. P. Chen, L. L. Ma, W. Hu, Z. X. Shen, H. K. Bisoyi, S. B. Wu, S. J. Ge, Q. Li, and Y. Q. Lu, "Chirality invertible superstructure mediated active planar optics," *Nat. Commun.* **10**(1), 2518 (2019).
15. T. Lin, Y. Yuan, Y. Zhou, W. Fu, H. Huang, L. Yao, F. Fan, and S. Wen, "Bragg reflective polychromatic vector beam generation from opposite-handed cholesteric liquid crystals," *Opt. Lett.* **44**(11), 2720–2723 (2019).
16. S. Y. Vetrov, M. V. Pyatnov, and I. V. Timofeev, "Photonic defect modes in a cholesteric liquid crystal with a resonant nanocomposite layer and a twist defect," *Phys. Rev. E* **90**(3), 032505 (2014).
17. N. Y. Ha, Y. Ohtsuka, S. M. Jeong, S. Nishimura, G. Suzuki, Y. Takanishi, K. Ishikawa, and H. Takezoe, "Fabrication of a simultaneous red–green–blue reflector using single-pitched cholesteric liquid crystals," *Nat. Mater.* **7**(1), 43–47 (2008).

18. M. E. McConney, V. P. Tondiglia, J. M. Hurtubise, L. V. Natarajan, T. J. White, and T. J. Bunning, "Thermally Induced, Multicolored Hyper-Reflective Cholesteric Liquid Crystals," *Adv. Mater.* **23**(12), 1453–1457 (2011).
19. A. H. Gevorgyan, "Photonic band gaps from a stack of right- and left-hand chiral photonic crystal layers," *Phys. Rev. E* **85**(2), 021704 (2012).
20. D. W. Berreman, "Optics in stratified and anisotropic media: 4×4 -matrix formulation," *J. Opt. Soc. Am.* **62**(4), 502–510 (1972).
21. Y. H. Huang, T. X. Wu, and S. T. Wu, "Simulations of liquid-crystal Fabry-Perot etalons by an improved 4×4 matrix method," *J. Appl. Phys.* **93**(5), 2490–2495 (2003).
22. S. T. Wu, "Birefringence dispersions of liquid crystals," *Phys. Rev. A* **33**(2), 1270–1274 (1986).
23. B. Wang, F. Dong, D. Yang, Z. Song, L. Xu, W. Chu, Q. Gong, and Y. Li, "Polarization-controlled color-tunable holograms with dielectric metasurfaces," *Optica* **4**(11), 1368–1371 (2017).
24. X. Zang, F. Dong, F. Yue, C. Zhang, L. Xu, Z. Song, M. Chen, P. Y. Chen, G. S. Buller, Y. Zhu, S. Zhuang, W. Chu, S. Zhang, and X. Chen, "Polarization encoded color image embedded in a dielectric metasurfaces," *Adv. Mater.* **30**(21), 1707499 (2018).
25. J. Deng, L. Deng, Z. Guan, J. Tao, G. Li, Z. Li, Z. Li, S. Yu, and G. Zheng, "Multiplexed anticounterfeiting meta-image displays with single-sized nanostructures," *Nano Lett.* **20**(3), 1830–1838 (2020).
26. C. Zhang, F. Dong, Y. Intaravanne, X. Zang, L. Xu, Z. Song, G. Zheng, W. Wang, W. Chu, and X. Chen, "Multichannel metasurfaces for anticounterfeiting," *Phys. Rev. Appl.* **12**(3), 034028 (2019).
27. F. Dong, H. Feng, L. Xu, B. Wang, Z. Song, X. Zhang, L. Yan, X. Li, Y. Tian, W. Wang, L. Sun, Y. Li, and W. Chu, "Information encoding with optical dielectric metasurface via independent multichannels," *ACS Photonics* **6**(1), 230–237 (2019).
28. D. Franklin, S. Modak, A. Vázquez-Guardado, A. Safaei, and D. Chanda, "Covert infrared image encoding through imprinted plasmonic cavities," *Light: Sci. Appl.* **7**(1), 93 (2018).
29. M. Schadt, H. Seiberle, and A. Schuster, "Optical patterning of multi-domain liquid-crystal displays with wide viewing angles," *Nature* **381**(6579), 212–215 (1996).
30. Y. Li, Y. Liu, S. Li, P. Zhou, T. Zhan, Q. Chen, Y. Su, and S. T. Wu, "Single-exposure fabrication of tunable Pancharatnam-Berry devices using a dye-doped liquid crystal," *Opt. Express* **27**(6), 9054–9060 (2019).
31. C. Oh and M. J. Escuti, "Achromatic diffraction from polarization gratings with high efficiency," *Opt. Lett.* **33**(20), 2287–2289 (2008).
32. Y. H. Lee, K. Yin, and S. T. Wu, "Reflective polarization volume gratings for high efficiency waveguide-coupling augmented reality displays," *Opt. Express* **25**(22), 27008–27014 (2017).